

A Computational Efficient Iris Extraction Approach in Unconstrained Environments

Yu Chen, Malek Adjouadi, Armando Barreto, Naphtali Rische, and Jean Andrian
College of Engineering and Computing, Florida International University, Miami, Florida 33174
Email: {ychen001, adjouadi, barretoa, rishe, andrianj}@fiu.edu

Abstract—This research introduces a noise-resistant and computational efficient segmentation approach towards less constrained iris recognition. The UBIRIS.v2 database which contains close-up eye images taken under visible light is used to test the proposed algorithm. The proposed segmentation approach is based on a modified and fast Hough transform augmented with a newly developed strategy to define iris boundaries with multi-arcs and multi-lines. This optimized iris segmentation approach achieves excellent results in both accuracy (2% error) and execution speed ($\leq 0.5s$ / image) using a 2.4GHz Intel® Q6600 processor with 2GB of RAM. This 2% error is an Exclusive-OR function in term of disagreeing pixels between the correct iris considered by the NICE.I committee and the segmented results from the proposed approach. The segmentation performance was independently evaluated in the “Noisy Iris Challenge Evaluation”, involving 97 participants worldwide, and ranking this research group in the top 6.

I. INTRODUCTION

BIOMETRIC research has experienced significant advances in recent years with the need for more stringent security requirements. After the first iris recognition system was proposed by J. Daugman in 1993, [1, 2] various commercial systems have since been developed to deal with eye images [3-6], which were mostly taken under rigorous acquisition scenarios. Under the current technological setups, to take an adequate iris picture, the subject must be still, look directly at the camera, and in a direction that satisfies very strict illumination conditions. This process is too constrained, time-consuming, and is often an inconvenience for the subject.[7,8] Thus, an effective iris recognition method is one that should initially overcome the rigid constraints imposed during iris image acquisition, and offer both acceptable accuracy and fast processing speed.[9-11]

Unconstrained iris recognition with less rigid image taking conditions can impose minimal to no constraints on the iris identification and verification process. To provide acceptable accuracy measures, it is critical for such iris recognition system to be complemented by a noise tolerant iris segmentation approach that overcomes various noises introduced through image capture under different recording environments and scenarios. [12- 15] Consequently, the focus of this work is on the development of a robust segmentation approach that can overcome such unpredictable noise effects in order to secure recognition outcomes with high accuracy.

The proposed algorithm consists of five steps, which

include: (1) detecting the approximate localization of the eye area of the noisy image captured at the visible wavelength, (2) defining the outer iris boundary which is the boundary between iris and sclera, (3) detecting the upper and lower eyelids, (4) conducting the outer iris boundary correction with multi-circle and multi-line, (5) detecting the pupil area and eyelashes.

The very challenging UBIRIS.v2 dataset, [16] which contains 500 eye images with realistic noisy effects, as provided by the University of Beira Interior, was used in this research. Two example images from the UBIRIS.v2 are shown in Figure 1(a) and (b), and are compared with example images from traditional dataset such as CASIA (version 3) [17] as illustrated in Figure 1(c) and (d). Note that the UBIRIS.v2 dataset images introduce more realistic conditions, such as specular reflections, off-angle situation and wearing of glasses as in these cases.

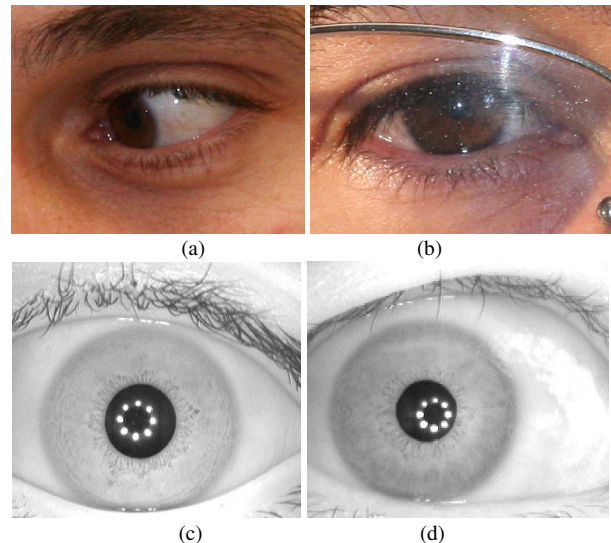


Fig. 1. Comparison of iris images from the UBIRIS.v2 and CASIA (version 3), (a), (b) two example images from the UBIRIS.v2, (c), (d) two example images from CASIA (version 3).

Three original contributions are made in this research endeavor: (1) a new iris segmentation approach which achieves excellent results in both accuracy and execution speed, (2) a newly developed strategy to define iris boundaries with multi-arcs and multi-lines, (3) a fast circular Hough transform is proposed to reduce the computation speed, which makes it more than 20 times faster. Such a modification is complemented with an optimization method designed to yield more accurate results.

II. APPROXIMATE LOCALIZATION OF THE EYE AREA

Irises from the UBIRIS.v2 database are extremely challenging to process, since they vary significantly in size and location because the images were taken with the subjects on the move and located at different distances (between 3 and 7 meters). The amount of pixels across the iris ranges from 75 to 190, and the iris may appear in any part of the close-up image. Therefore, as an initial step of the proposed approach, a method is used to approximately localize the eye part of the image in order to obtain a smaller and more refined target area. This method, which is of considerable benefit in seeking accuracy and fast processing speed for segmentation purposes, consists of two steps: (1) finding an approximate eye area based on sclera detection, and (2) determining an adaptive target region to confine the search for the iris.

A. Detecting the sclera area

Since the iris may appear in any part of the close-up image, most existing iris segmentation approaches start from pupil detection because the pupil area is the darkest part; those images considered are captured under NIR (near-infrared) wavelength with rigidly constrained environments. However, all the close-up images are full-color images taken under visible wavelengths. Under this condition, the pupil area may not always appear darker than other parts, especially for images containing heavily pigmented (dark) irises, or images affected by noise. Thus, pupil detection is no longer the appropriate first step when localizing the eye area. Through analyzing the full-color images, the sclera part is found to be less saturated (white) than other parts of the images. Consequently, the proposed approach starts from the sclera detection to determine the target eye area.

As the non-constrained iris images are taken without rigid illumination control, their processing requires overcoming intricate lighting conditions such as uneven lighting, reflections, and shadows. In this study, the hue, saturation and intensity, the HSI color model, is used to detect the sclera instead of the RGB model. The saturation value of the HSI model refers to the degree of white which is added to the color. Furthermore, the HSI model decouples the intensity component from the color-carrying information (hue and saturation values). [18]

Through our experimental analysis, the saturation values of sclera areas range from 0 to 0.21(0 to 54, with a normalized range from 0 to 255). The saturation value, which refers to the sclera, would be calculated as a threshold, and all pixels below the threshold would be considered as pixels belonging to the sclera. An adaptive threshold is thus obtained by calculating the biggest group derivative within the range in a histogram of saturation values (between 0 and 54) corresponding to the image. The process for obtaining the saturation threshold value consists of making use of equations (1-4) as follows:

$$G_j = \sum_{i=0}^{M-1} (S_{j+i}), \text{ where } 0 \leq j \leq 54 \quad (1)$$

$$D_j = (G_{j+\varepsilon} - G_j) / G_{j+\varepsilon} \quad (2)$$

$$H_j = \sum_{i=0}^{N-1} (D_{j+i}) \quad (3)$$

$$T_j = \text{Max}(H_j) \quad (4)$$

Here, S_j is the amount of pixels which have the saturation value j , on the saturation histogram of the eye image. D_j is the group derivative for every M neighboring saturation values of the saturation histogram (here, $M=14$). The value $\varepsilon = 2$ is chosen empirically as means to seek relevant first derivatives on the basis of the smoothed saturation histogram by using equation (1). The saturation value threshold j of T_j is obtained by searching for the maximum smoothed group derivative value H_j ,

Two eye images with different luminous intensities are illustrated in Figure 2. Figure 2(e) and Figure 2(f) display two results of extracting the sclera pixels from all other pixels, with the inherent noise points which would be resolved in the subsequent processing step.

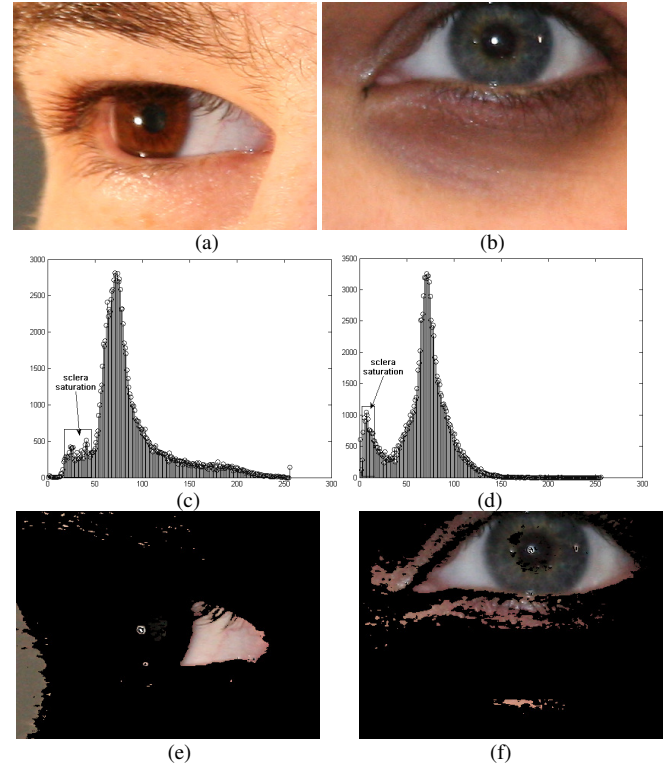


Fig. 2. Sclera detection under different lighting conditions, (a) eye image with high luminous intensity, (b) eye image with low luminous intensity, (c), (d) saturation histograms for the corresponding eye images, (e), (f) sclera detection results.

B. Determining a target area for the eye

Since the sizes of irises vary significantly, the purpose of this step is to locate a target area with an adaptive size in order to adjust for the different irises. After the sclera detection step, it can be observed that some small spots of reflections and bright skin are scattered on the image as part of the sclera extraction result. Thus, more specific sclera areas need to be

localized first to overcome/eliminate the noise points. In opposition to the sclera part, all other spots are generally smaller or slightly darker. The sclera detection images as in Figure 2(e) and Figure 2(f) are converted to grayscale images, and for every pixel with gray level intensity greater than 0, its value will be replaced by the average intensity value of a 17 by 17 block which is centered on that pixel. With this operation, the intensities of isolated and relatively smaller noise areas would be degraded significantly. For those pixels whose gray level intensities are greater than 0, the average intensity is calculated to be an adaptive threshold. With this threshold, a binary map, which can clearly specify the sclera area, can be generated.

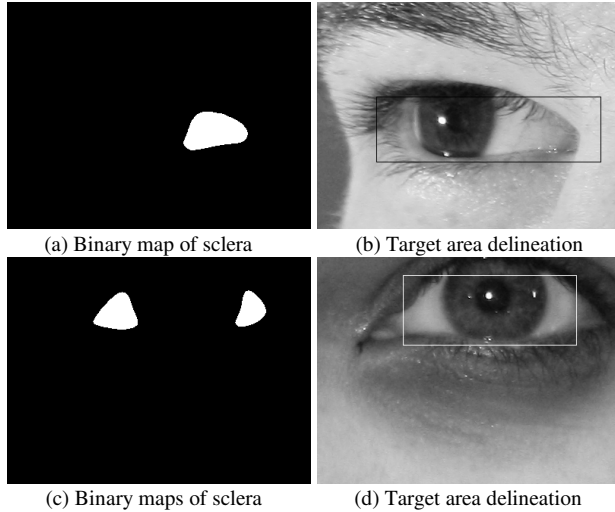


Fig. 3. Target selection for the eye area based on double and single sclera areas.

The resulting binary maps can be classified into two categories: single sclera area as shown in Figure 3(a), which corresponds to Figure 2(a), and double sclera areas as shown in Figure 3(c), which corresponds to input image Figure 2(b).

With a single sclera area as shown in Figure 3(a), it is unknown which side of sclera the iris will be located in. The nearest distances between the sclera area to the left and right boundaries of the image would be calculated, respectively. The rectangular area would be decided with respect to those distances. The longer the distance, the more the rectangle would be extended towards the boundary in that direction. As shown in Figure 3(b), the resulting rectangle (shown in black) was mostly extended towards the left side, and as a result the iris part is within the rectangle, which correctly delineates the target area.

With double sclera appearing, the iris would certainly be located between them. The rectangular area can be determined by the extreme coordinates of upper, lower, left and right locations of the two sclera areas. In order to ensure inclusion of the entire iris, the rectangle would be enlarged with an offset proportional to the distance between extreme points in relation to the image boundaries. As shown in Figure 3(d), the target rectangle (shown in white) covers most of the iris.

III. DETECTING IRIS OUTER BOUNDARY WITH A FAST CIRCULAR HOUGH TRANSFORM

The outer boundary of the iris is defined as the boundary between iris and sclera. Hough transform is tolerant of gaps in edge descriptions and is relatively unaffected by image noise.

A. Detecting the outer boundary

To generate the edge map, instead of the traditional four-direction Sobel edge detection, we only conduct the edge detection horizontally (left to right and right to left).[19, 20] The number of edge points in figure 4 (b), which was generated using 4 directions edge detection, was much reduced from that of figure 4 (c).

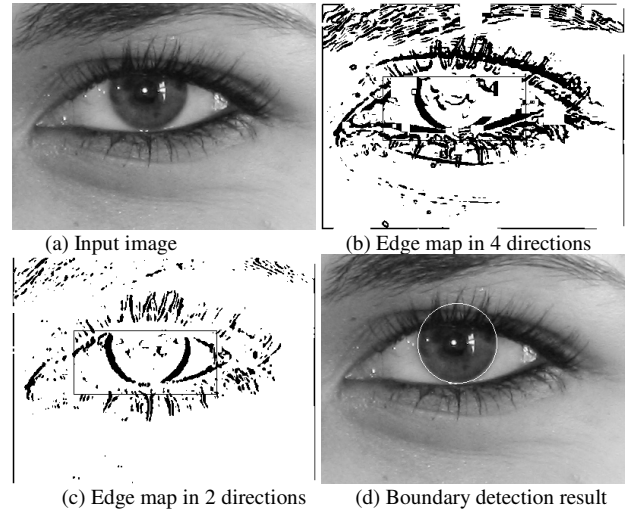


Fig. 4. Example of outer boundary detection using the modified circular Hough transform.

Based on the information obtained from the previous step, to improve the accuracy and processing speed, after generating the edge map, the circular Hough transform would only be conducted using the edge points in the target rectangle. Also, some precautions are considered. First, the upper and lower limits of the radius can be set with respect to the size of rectangle. Thus, the upper limit of the radius is set as $1/2$ of the rectangle's length, and the lower limit is set as $1/4$ of the rectangle's width. Second, neither the center of the resulting circle nor its boundary can possibly be located on the already defined sclera areas.

B. A fast circular Hough transform

Although the circular Hough transform is a powerful algorithm, it also carries with it a heavy computational accumulator which refers to the three step iterations burden. With the circular Hough transform, each edge point (x, y) in the image space votes for each possible circle represented as (a, b, r) in the parameter space, And a, b are the coordinates of the circle center position, and r being the radius of the circle. Thus, the votes were cast in a three directions accumulator for conducting the transform. [21] If Q_1 is the computational complexity of calculating votes for a circle

with a determined center location and radius, the computational complexity of the circular Hough transform Q_a would be as given by equation (5):

$$Q_a = (a_{\max} - a_{\min}) * (b_{\max} - b_{\min}) * (r_{\max} - r_{\min}) * Q_1 \quad (1)$$

Here the step-length was applied to reduce the computational burden of the circular Hough transform. If C_a , C_b , and C_r are the step-length for parameters a, b, and c respectively, then the computational complexity would be as given by equation (6):

$$Q_b = (a_{\max} - a_{\min}) * (b_{\max} - b_{\min}) * (r_{\max} - r_{\min}) * Q_1 / (C_a * C_b * C_r) \quad (2)$$

Because of the three step-lengths, a large number of votes will not be counted. To overcome this problem, with a determined circle center and radius, instead of only searching for the edge points located on the circle, all points located on the circular ring surrounding that circle would be counted. For instance, as shown in Figure 5, instead of searching for edge points located on the solid circle 1, the search will also include all points within the dashed circles A and B; similarly, all points within dashed circle B and C would count as votes for the target searching circle given by solid circle 2.

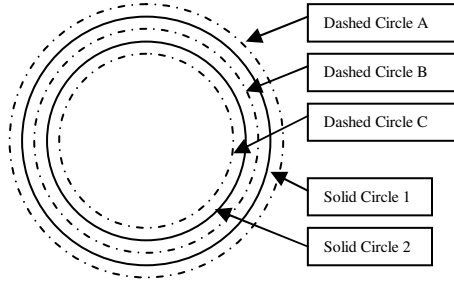


Fig. 5. Example of searching feature points located on the circular ring around the target circle.

To accelerate the step of searching for all the edge points located on the circular rings, we implement the algorithm with the dynamic programming method. Initially, the distance between every pixel point on the image and the image center point would be calculated; all those distances would be stored as a look-up table, and each distance would refer to a list of relative locations which have that certain distance from the center location of the image. Thus, when searching for the edge points on the circle, the neighboring distances would refer to a set of relative locations in the look-up table, and all edge points located on the corresponding locations in the image would be counted. Because the look-up table was generated just after executing the proposed approach for a single image, and since the size of all input images is 400 by 300, there is no need to calculate distances while performing the Hough transform for each image. The computational burden was consequently alleviated significantly.

The step-length is set to be between 1 and 5. The processing time is examined by processing the 500 iris images from the UBIRIS.v2 database using a computer station with 2.4GHz CPU (Intel® Q6600) and with 2GB of RAM. The results are as shown in Figure 6, where the step-length for C1

through C5 are 1 though 5, respectively. In this study, a step-length of 5 is used to optimize the processing time of the Hough circular transform, while preserving the accuracy of the results. This makes it more than 23.2 times faster than the approach using a step-length of 1.

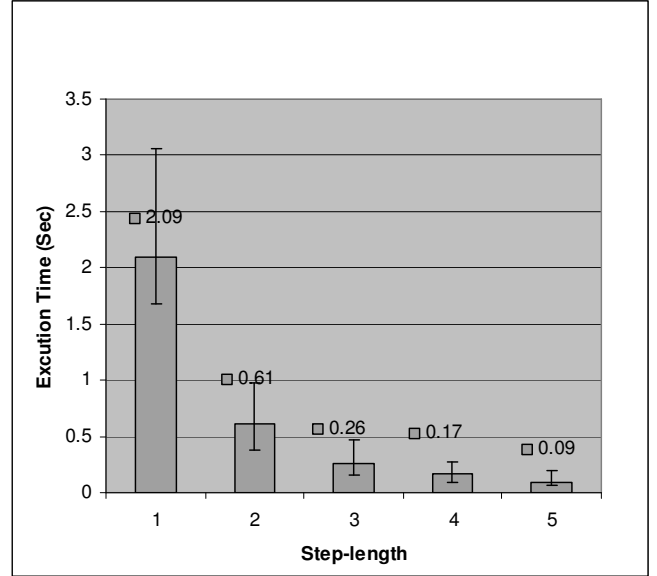


Fig. 6. Average processing time for circular Hough transform.

Without using the optimized step-length method, the average processing time per image is 2.09 secs for circular Hough transform and 2.68 for the proposed approach, and the segmentation error rate of such an approach is determined to be 0.0200215.

The segmentation error rate is obtained using an Exclusive-OR function in terms of disagreeing pixels between the correct iris considered by the NICE.I committee and the results generated by the proposed approach (executable).

For each input iris image I_i , O_i is the output segmented binary iris image generated by the participant, C_i is the classified (standard) binary iris image provided by NICE.I Committee. The error rate as used in this study was computed using the following equation:

$$E_i = \frac{1}{c * r} \sum_{c'} \sum_{r'} O_i(c', r') \otimes C_i(c', r') \quad (3)$$

where $O_i(c', r')$ and $C_i(c', r')$ are pixels of the output and classified binary iris map, respectively.

$$E = \frac{1}{n} \sum_i E_i \quad (4)$$

The proposed method decreases the execution time of the proposed approach significantly and does not bring notable increase in the segmentation error of the proposed approach. With the proposed modified circular Hough transform, the average execution time for the proposed approach is decreased to 0.39 sec and the error rate is 0.0200823. Compared with not using the optimized step-length method, the execution time for the proposed approach is significantly decreased by 6.9 times, and the accuracy is only degraded by 0.303%, which is considered negligible.

C. Detecting the boundary of the eyelids

For unconstrained iris recognition, because the subject is not required to comply with a demanding level of cooperation, it is observed that eyelid occlusion often occurs. Thus, the third step focused on detecting the upper and lower eyelids. A Hough line transform is used recursively to extract edges of eyelids. Illustrative results are shown in Figure 7.

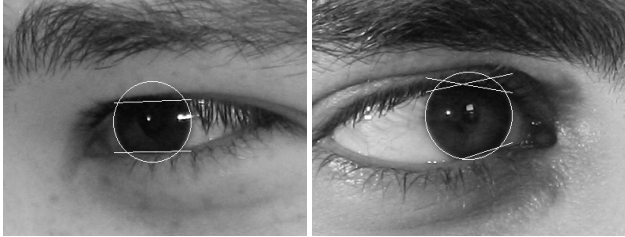


Fig. 7. Results of eyelid boundary detection using two subjects.

IV. CIRCLE CORRECTION AND NON-CIRCULAR BOUNDARY DETECTION

Although the outer iris boundary was assumed to be circular for most of the conventional iris segmentation methods, it has been pointed out that human iris boundaries are usually non-circular. The errors caused by defining the boundary as circles are especially crucial for less constrained iris recognition, because a considerable portion of iris images with off-angle effects will usually be generated under the non-cooperative iris acquisition scenarios. Two examples of off-angle iris images are given in Figure 8. The white circles shown in two images of Figure 8 indicate the results of circular Hough transform for outer iris boundary detection. As can be seen, traditional circular iris outer boundary detection would be inadequate to process the iris images with non-circular boundary effects. Also the circular Hough transform can generate inaccurate results due to noise. Thus, a strategy was developed to define the non-circle boundary and correct the inaccurate result obtained from the circular Hough transform.

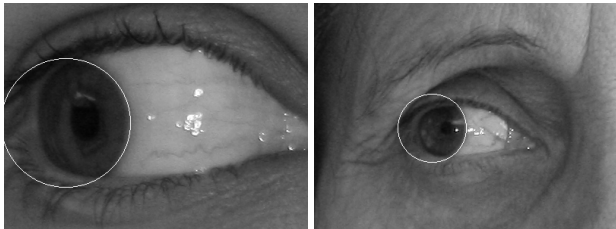


Fig. 8. Examples of non-circular iris boundaries and error results of original outer iris boundary detection, shown as the white circles.

Figure 9(a) is one example of outer boundary detection error caused by a non-circular iris boundary. As can be seen, the outer boundary cannot be correctly detected. The proposed verification and correction method is based on two steps; the first is the circle center verification, the second is multiple circle (or arc) searching, and multiple arcs and lines connection.

There is a need to find the correct center of the iris to verify the original circle center found from the first circle Hough

transform. Shown in Figure 9(b) is a square grid with an adaptive sized inside the outer iris boundary.

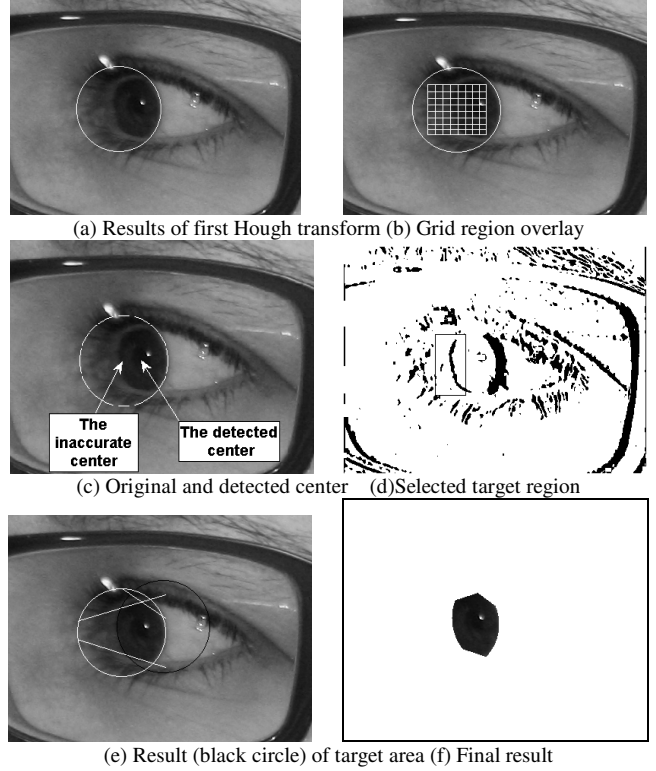


Fig. 9. Defining the noncircular iris boundary

The center of the grid which yields the lowest average gray intensity would be selected as the correct outer iris boundary center. If the difference between the original center and the newly detected one is greater than $R_{outer} / 4$, the original outer boundary would be assumed to be inaccurate. Then a target area would be selected for conducting Hough circular transform again. Empirically, the desired iris boundary is usually inside the Hough circle. This is because the edge points outside the iris usually vote for a larger circle and for an off-angle iris which is smaller than its actual size. Thus, the target area whose center is at (x_t, y_t) as shown in Figure 10 was expected to be the region between the real iris center (x_r, y_r) and the arc on the opposite side of the original circle. In reference to Figure 10, the center of the target rectangle is (x_t, y_t) , and the original circle center is (x_c, y_c) , where:

$$y_t = y_c \text{ and } x_t = x_c - (x_r - x_c) \text{ or } x_t = 2x_c - x_r \quad (5)$$

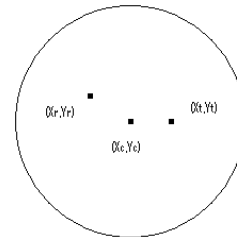


Fig. 10. Relations between the real iris center, original circle center and center for target rectangle.

Another Hough transform will be conducted to the edge points inside the target rectangle. The black circle shown

earlier in Figure 9(e) is one outcome example of this step.

The intersection of two circles could be used to describe the noncircular iris. The upper and lower eyelid lines would also be used to remove unexpected eyelids and eyelashes. Figure 9 (f) illustrates the final result of the detected boundary consisting of multiple arcs and lines, and would be much more accurate for describing non-circular iris boundaries. Other examples are shown in Figure 11.

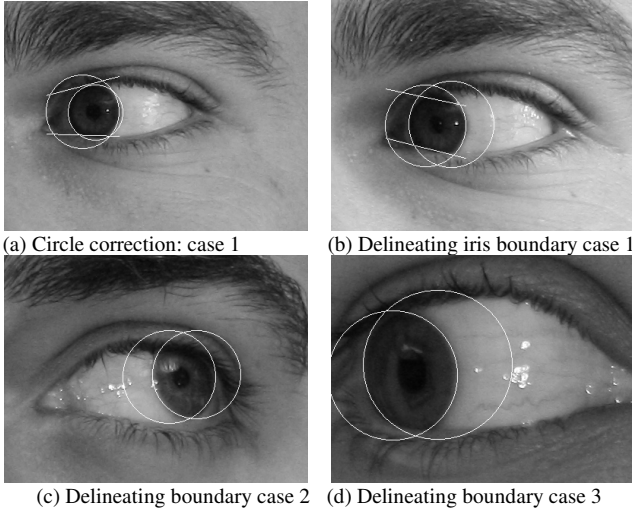


Fig. 11. Results of circle verification and correction strategy for delineating non-circular iris boundaries.

Inaccuracies introduced by the circular Hough transform are resolved with the proposed method. As shown in Figure 11, the larger circle in (a) is an inaccurate circular Hough transform result, and the smaller circle is the newly detected version through the proposed method. Figure 11(b)-(d) are examples with off-angle iris images with different iris sizes and different eye gazes. The left circles shown in Figure 11 (b)-(c) and the right circle shown in Figure 11(d) are the original Hough transform results, which are considerably off from the expected results. But as can be seen, the intersections are much more accurate.

V. PUPIL AND EYELASH DETECTION

Because the eye images from the UBIRIS.v2 dataset were captured under visible wavelengths, one of the major differences with those images taken under NIR illumination is that the intensity contrast of iris and pupil can be very low, especially for heavily pigmented (dark) irises, such as in Figure 12(a). Thus, pupil removal is left to be performed during this step; with only iris and pupil appearing, the contrast enhancement method would yield better performance.

As shown in Figure 12, image (a) is the outcome from the previous step (outer iris and upper and lower eyelid boundary delineation). We used an empirical intensity threshold of 150 to detect the reflections, and a 3 by 3 mask is used to detect and remove all the pixels within the iris and pupil boundaries that exceed this set threshold. Then, histogram equalization was applied to get the high-contrast image, as shown in image (b). Sobel edge detection was used to get the edge map (c), and then the circular Hough transform determined the pupil

boundary. Caution is taken such that the pupil center should be located within the small white circle shown in Figure 12(b) with a radius of $R_{outer} / 10$, and its center can be considered as the outer iris center. The radius of the pupil boundary is set to be from $3R_{outer} / 20$ as a lower limit, to $11R_{outer} / 20$ as the upper limit. Those predefined parameters are based on the experimental analysis on the target database. Figure 12(d) shows the result for this example.

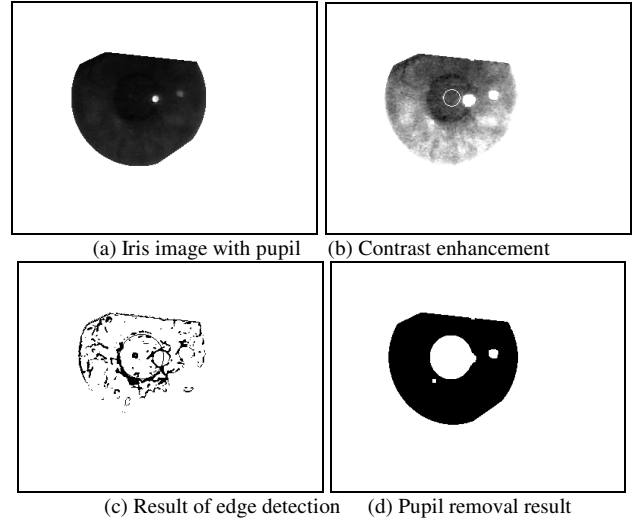


Fig. 12. Process for pupil detection and removal.

To detect the eyelashes, we set an adaptive empirical threshold to be $0.45 * I_A$, where I_A is the obtained average gray intensity of the iris. The eyelash removal would be performed within the top $R_{outer} / 3$ part of the iris. After the pupil and eyelash removal, the result of the segmentation approach would be generated.

VI. RESULT AND EVALUATION

The error rate is estimated at 2.0% using 500 images from the UBIRIS.v2 database, and was estimated at 2.9% by NICE.I committee with a much larger portion of the database UBIRIS.v2. The result ranked us in the top 6 among 97 participants/teams worldwide (from 34 countries). [22]

Through evaluation, the worst results were caused by sclera detection errors, as shown in Figure 13(a). For this image, the sclera area was found to be the bright part of the upper eyelid, with the target rectangle falsely set to be out of iris region. Figure 13(b) shows that, with an incorrect searching target area, unpredictable results would be obtained from the circular Hough transform. The black circle on the top-right of the image is the outcome of iris boundary detection conducted in the non-iris region.

As for the example in Figure 13(c), because the white wall behind the subject is wrongly detected to be sclera, the target rectangle is set to be too large for the actual iris region to be detected. Therefore, the upper limit radius of the target circle was set to be too large as well. (recall that the upper limit of the radius is set to be half of the rectangle length in the proposed approach). As shown in Figure 13(d), a very large

circle can get more votes than the actual boundary circle, resulting in incorrect segmentation.

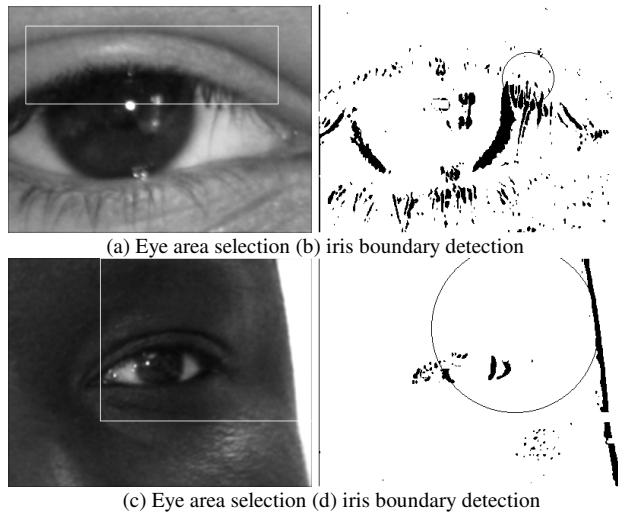


Fig. 13. Examples yielding faulty or undesired results.

VII. CONCLUSION

This study proposed a noise-resistant and fast approach for iris segmentation based non-constrained iris recognition. It produces high performance in the eye images from the UBIRIS.v2 database which contains very realistic noise effects. This accuracy is augmented in merit because the processing speed of the proposed approach is near-real-time, requiring only 0.39sec per image to perform all the required steps for final iris segmentation. The proposed approach relies on an effective search for the sclera area of the image. A threshold of saturation value, the HSI color model, is obtained by calculating the biggest group derivative of the original color image histogram. A binary map was then generated to indicate the sclera area. The proposed method determines a more refined target area in order to accelerate the circle searching for the outer iris boundary. The outer boundary of the iris was detected using a fast and accurate modified circular Hough transform. The linear Hough transform is then used recursively to extract edges of eyelids.

A new method of verification and correction for the outer iris boundary was also proposed. This method is based on the iris center correction, and a regional circular Hough transform. Multiple arcs and lines can thus be used to describe an iris boundary, and the non-circular iris boundary would be described correctly. The pupil and eyelashes are detected in the final step using the Sobel edge operator on the histogram-equalized iris image.

ACKNOWLEDGMENT

The authors appreciate the support provided by the National Science Foundation under grants HRD-0833093, CNS-0426125, CNS-0520811, and CNS-0540592.

REFERENCES

- [1]. J. Daugman, "High Confidence Visual Recognition of Persons by a Test of Statistical Independence", IEEE, PAMI, Vol.15, No 11, pp. 1148-1161, 1993.
- [2]. R.P. Wildes. Iris recognition: An emerging biometric technology. Proceedings of the IEEE, 85(9):1348-1363, 1997.
- [3]. L. Ma, T. Tan, Y. Wang, and D. Zhang. Personal identification based on iris texture analysis. IEEE Trans. on PAMI, 25(12):1519-1533, 2003.
- [4]. Z. He, Z. Sun, T. Tan, X. Qiu, C. Zhong, W. Dong, Boosting ordinal features for accurate and fast iris recognition, Computer Vision and Pattern Recognition, 2008. CVPR 2008. IEEE Conference on 23-28 June 2008 Page(s):1 - 8, DOI: 10.1109/CVPR.2008.4587645
- [5]. S.A.C. Schuckers, N.A. Schmid, A. Abhyankar, V. Dorairaj, C.K. Boyce and L.A. Hornak, "On techniques for angle compensation in nonideal iris recognition", IEEE Trans. SMC-B 37(5), pp.1176-1190 (2007)
- [6]. A.K. Jain, P.J. Flynn and A.A. Ross, "Handbook of Multibiometrics", ISBN: 9780387710402, Springer, 2006.
- [7]. H. Proença, L.A. Alexandre, Toward non-cooperative iris recognition: a classification approach using multiple signatures, IEEE Trans. Pattern Anal. Mach. Intell. 29 (4) pp. 607-612, 2007.
- [8]. J.R. Matey, O. Naroditsky, K. Hanna, R. Kolczynski, D. Lolocono, S. Mangru, M. Tinker, T. Zappia, W.Y. Zhao, "Iris on the Move : acquisition of images for iris recognition in less constrained environments", Proc. of the IEEE, 94 (11), pp. 1936-1946, 2006.
- [9]. J. Daugman, "How iris recognition works", IEEE Trans. Circ. Syst. Video Technol. 14 (1), pp. 21-30, 2004.
- [10]. R. Hamza, R. Whillock, "Standoff iris recognition using non-iterative polar based segmentation", Proc. SPIE, Vol. 6944, 694405 (2008); DOI:10.1117/12.777206, Biometric Technology for Human Identification V, 18 March 2008, Orlando, FL, USA.
- [11]. Y. Chen, J. Wang, and M. Adjouadi, "A Robust Segmentation Approach to Iris Recognition Based on Video", Proc. of IEEE-AIPR, pp.1-8, ISBN: 978-1-4244-3125-0, Washington DC, Oct. 15-17, 2008.
- [12]. E. Newton, P. J. Phillips, "Meta-analysis of third party evaluations of iris recognition", in: Biometrics: Theory, Applications, and Systems, Sept 2007, 1-4.
- [13]. Y. Chen, M. Adjouadi, C. Han, J. Wang, A. Barreto, N. Rische, J. Andrian, A Highly Accurate and Computationally Efficient Approach for Unconstrained Iris Segmentation, Image and Vision Computing (2009), doi: 10.1016/j.imavis.2009.04.017.
- [14]. N.A. Schmid, M. Ketkar, H. Singh and B. Cukic, "Performance Analysis of Iris-Based Identification System at the Matching Score Level", IEEE Trans. on Information Forensics and Security, vol. 1, (2006), p. 154.
- [15]. X. Liu, K.W. Bowyer and P.J. Flynn. "Experimental evaluation of iris recognition", Proc. of Face Recognition Grand Challenge Workshop, 2005, III: 158-165.
- [16]. H. Proença and L.A. Alexandre. Ubiris iris image database, <http://iris.di.ubi.pt>. 2004.
- [17]. CASIA iris image database, <http://www.sinobiometrics.com/casiairis.htm>.
- [18]. L. Sigal, S. Sclaroff and V. Athitsos, "Skin Color-Based Video Segmentation under Time-Varying Illumination" IEEE Trans. on PAMI, 26(7):862-877, July, 2004.
- [19]. M. Adjouadi and F. Candocia, "A Stereo Matching Paradigm Based on the Walsh Transformation", IEEE PAMI, Vol. 16, No. 12, pp. 1212-1218, Dec. 1994.
- [20]. M. Adjouadi, F. Candocia, X. Zhang and J. Riley "Exploiting Walsh-Based Attributes in Stereo Vision", IEEE Trans. on Signal Proc., Vol. 44, No. 2, pp. 409-420, February 1996.
- [21]. Y. Chen, M. Adjouadi, C. Han and A. Barreto "A new unconstrained iris image analysis and segmentation method in biometrics", IEEE International Symposium on Biomedical Imaging, ISBI, Boston, MA, U.S.A., Jun 28-Jul 1, 2009, pp.13-16, DOI: 10.1109.
- [22]. H. Proença, L. A. Alexandre; The NICE.I: Noisy Iris Challenge Evaluation - Part I, Proc. of the IEEE 1st International Conf. on Biometrics: Theory, Applications and Systems - BTAS, Washington DC, U.S.A., Sep. 27-29, 2007, ISBN: 978-1-4244-1597-7.